J. Opt. **14** (2012) 085501 (6pp) doi:10.1088/2040-8978/14/8/085501

Fabrication and characterization of compact silicon oxynitride waveguides on silicon chips

Lianghong Yin[1,5], Ming Lu[2], Leszek Wielunski[3,4], Weiwei Song[1], Jun Tan[1], Yicheng Lu[1,4] and Wei Jiang[1,4]

[1] Department of Electrical and Computer Engineering, Rutgers University, Piscataway, NJ 08854, USA
[2] Center for Functional Nanomaterials, Brookhaven National Laboratory, Upton, NY 11973, USA
[3] Laboratory for Surface Modification, Rutgers University, Piscataway, NJ 08854, USA
[4] Institute for Advanced Materials, Devices, and Nanotechnology, Rutgers University, Piscataway, NJ 08854, USA

E-mail: wjiangnj@rci.rutgers.edu

Received 28 April 2012, accepted for publication 4 July 2012
Published 1 August 2012
Online at stacks.iop.org/JOpt/14/085501

Abstract
We investigate silicon oxynitride (SiON) waveguides for long optical delay lines on a silicon chip. With the choice of a moderately low refractive index contrast, a balance can be achieved between compact waveguide cross-section and low loss. The material composition and refractive index are characterized by Rutherford backscattering spectrometry and ellipsometry. High-temperature annealing is performed after waveguide fabrication so as to simultaneously remove light absorbing bonds in the materials and smooth the sidewall roughness at the core–cladding interface. A meter-long SiON waveguide is demonstrated on a centimeter scale chip.

Keywords: silicon oxynitride, optical delay lines, spiral waveguide

(Some figures may appear in colour only in the online journal)

1. Introduction

Silicon photonics has emerged in the last few years as a promising platform for optical device integration in a wide range of applications [1–3]. Significant progress has been made in silicon based modulators, photodetectors, amplifiers, lasers, and nonlinear optical devices [4–11]. There has been a continuing interest in developing other photonic devices on the silicon platform to enable new applications for silicon photonics. Optical delay lines have important applications in phased array antennas [12, 13] and optical buffers used for optical networking [14, 15]. Compared to conventional fiber-optic delay lines, integrated waveguide delay lines have a compact form factor and obvious on-chip integration advantage. Silicon compatible on-chip optical delay lines are especially attractive as they can be seamlessly integrated with other silicon photonic devices to form an on-chip optical interconnect system or an on-chip switchable delay network (for phased array antennas).

Many silicon compatible materials, including silicon itself, silica, and silicon nitride, have been investigated for integrated optical delay lines [14–18]. Silicon oxynitride (SiON) is a promising candidate to serve as the core material of on-chip delay lines. SiON is compatible with Si very-large-scale integration (VLSI) technology and can be readily integrated with other silicon photonic devices in delay-line related applications. With SiO_2 cladding, SiON waveguides can potentially have significantly lower loss than silicon waveguides. Waveguide theory predicts that the scattering loss of an optical waveguide due to random interface roughness is proportional to $(n_1^2-n_2^2)^2$ and σ^2, where n_1 and n_2 are the refractive indices of the core and cladding

[5] Present address: GLOBALFOUNDRIES, 2070 Route 52, Mail Drop A10, Hopewell Junction, NY 12533, USA.

Report Documentation Page			Form Approved OMB No. 0704-0188
Public reporting burden for the collection of information is estimated to average 1 hour per response, including the time for reviewing instructions, searching existing data sources, gathering and maintaining the data needed, and completing and reviewing the collection of information. Send comments regarding this burden estimate or any other aspect of this collection of information, including suggestions for reducing this burden, to Washington Headquarters Services, Directorate for Information Operations and Reports, 1215 Jefferson Davis Highway, Suite 1204, Arlington VA 22202-4302. Respondents should be aware that notwithstanding any other provision of law, no person shall be subject to a penalty for failing to comply with a collection of information if it does not display a currently valid OMB control number.			
1. REPORT DATE **01 AUG 2012**	2. REPORT TYPE		3. DATES COVERED **00-00-2012 to 00-00-2012**
4. TITLE AND SUBTITLE **Fabrication and characterization of compact silicon oxynitride waveguides on silicon chips**			5a. CONTRACT NUMBER 5b. GRANT NUMBER 5c. PROGRAM ELEMENT NUMBER
6. AUTHOR(S)			5d. PROJECT NUMBER 5e. TASK NUMBER 5f. WORK UNIT NUMBER
7. PERFORMING ORGANIZATION NAME(S) AND ADDRESS(ES) **Rutgers University,Department of Electrical and Computer Engineering,Piscataway,NJ,08854**			8. PERFORMING ORGANIZATION REPORT NUMBER
9. SPONSORING/MONITORING AGENCY NAME(S) AND ADDRESS(ES)			10. SPONSOR/MONITOR'S ACRONYM(S) 11. SPONSOR/MONITOR'S REPORT NUMBER(S)
12. DISTRIBUTION/AVAILABILITY STATEMENT **Approved for public release; distribution unlimited**			
13. SUPPLEMENTARY NOTES			
14. ABSTRACT **We investigate silicon oxynitride (SiON) waveguides for long optical delay lines on a silicon chip. With the choice of a moderately low refractive index contrast, a balance can be achieved between compact waveguide cross-section and low loss. The material composition and refractive index are characterized by Rutherford backscattering spectrometry and ellipsometry. High-temperature annealing is performed after waveguide fabrication so as to simultaneously remove light absorbing bonds in the materials and smooth the sidewall roughness at the core?cladding interface. A meter-long SiON waveguide is demonstrated on a centimeter scale chip.**			
15. SUBJECT TERMS			

16. SECURITY CLASSIFICATION OF:			17. LIMITATION OF ABSTRACT	18. NUMBER OF PAGES	19a. NAME OF RESPONSIBLE PERSON
a. REPORT **unclassified**	b. ABSTRACT **unclassified**	c. THIS PAGE **unclassified**	**Same as Report (SAR)**	**6**	

Standard Form 298 (Rev. 8-98)
Prescribed by ANSI Std Z39-18

materials, and σ is the rms surface roughness [19, 20]. SiON waveguides have substantially lower index contrast than silicon waveguides. Thus they tend to produce substantially lower loss, which allows for much longer optical delays. Compared to Ge-doped SiO_2, SiON provides a much larger index tuning range due to the high refractive index of the nitride component. This offers significant flexibilities in tailoring the index contrast for different applications. Note that silicon nitride itself has been investigated for various waveguide applications [18, 21]. Compared to pure silicon nitride, the capability of varying the ratio of oxygen and nitrogen in SiON also offers significant design flexibility for suiting the needs of different applications. An excellent overview of SiON waveguides for optic communications applications can be found in [22]. Note that SiON waveguides have been employed in devices such as filters, dispersion compensators, ring resonators, and optical switches [22–24]. For these devices, SiON waveguides with relatively large cross-sections and relatively short lengths (centimeters) were used. However, to explore the on-chip delay-line application in the regime of nanoseconds, single mode SiON waveguides with small cross-sections and meter-scale lengths are needed to fit in a small chip.

In this work, we experimentally investigate SiON waveguides in a design regime that can offer lower loss than Si based delay lines yet maintain a reasonably compact cross-section. Whereas SiON waveguides may have limited applications in optical switches and resonators in comparison to Si based active devices, due to size and power consumption issues, delay lines could open up a promising new direction for SiON waveguides due to their lower loss, wider tunability of the refractive index, and excellent compatibility with the Si VLSI technology.

2. Film deposition and characterization

First, we deposit SiON thin films with varying nitrogen concentrations using a plasma enhanced chemical vapor deposition (PECVD) system (Trion Orion III) and characterize their refractive indices and compositions. Starting with a standard SiO_2 recipe, we add the gas NH_3. Through changing the flow rate of NH_3, SiON films with refractive indices from 1.447 to 1.651 (at $\lambda = 1.55$ μm) are obtained, as shown in figure 1.

The refractive indices and thicknesses of the films on silicon substrates are measured by a broadband spectroscopic ellipsometer (J A Woollam M-2000). The relationship of the index versus the flow rate ratio $r = NH_3/(SiH_4+NH_3+N_2O)$ is close to linear, as shown in figure 1. Further, we employ Rutherford backscattering spectrometry (RBS) to characterize the atomic percentage of nitrogen inside the material. The Rutgers Tandem Accelerator provides 2 MeV He^{2+} ions as a primary ion beam for RBS. A typical surface-barrier silicon detector is used for scattered ion detection and a PC based multichannel analyzer is used for RBS spectrum collection. RBS data are analyzed using the commercial program SIMNRA. Three samples deposited at the flow rate ratios $r = 18\%$, 40%, and 76% are characterized by RBS. Silicon, oxygen, and nitrogen atomic percentages are obtained from optimal fitting for the RBS spectra using SIMNRA. From the RBS data, SIMNRA gives the ratio of nitrogen and oxygen atomic percentages in these films as (N at.%)/(O at.%) = 0.13, 0.42, and 1.13 respectively.

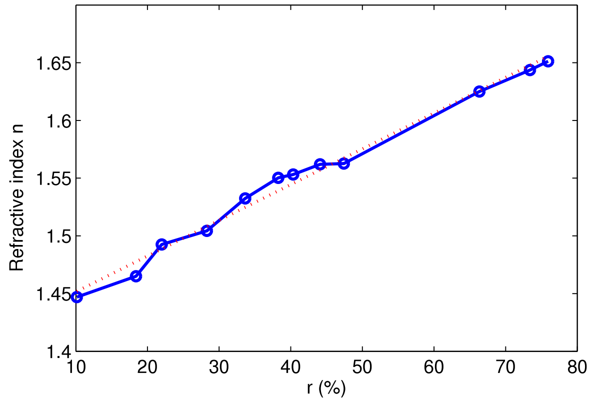

Figure 1. Refractive index of SiON film as a function of the ratio $r = NH_3/(SiH_4 + NH_3 + N_2O)$ (percentage).

3. Fabrication

In this part, we present the structure of SiON waveguides and the detailed fabrication processes. For these waveguides, we deposit SiON films with the flow rate ratio $r = 44.1\%$ to obtain a refractive index of 1.562 at 1.55 μm. Our experimental results presented below show that this choice of refractive index contrast (of the order of 0.1) finds a balance of small waveguide cross-sections, low propagation loss, and small bending loss in a reasonably small bending radius. Suppose an SiON waveguide consists of a 0.9 μm thick core ($n = 1.562$) surrounded by SiO_2 ($n = 1.445$); the maximum width for such a waveguide operating in the single mode regime (TE polarization) at $\lambda = 1.55$ μm is found to be 2.5 μm by MATLAB based finite difference in frequency domain (FDFD) simulations [25]. Since SiON has a lower refractive index than the Si substrate, a fairly thick SiO_2 layer is needed to prevent light leaking into the Si substrate. The FDFD simulation shows that the amplitude of the major component of the electrical field decreases by 6×10^{-6} at a distance of 6 μm from the bottom of the waveguide core. So a 6 μm thick SiO_2 underlayer should suffice for our purpose.

We deposit a 0.9 μm thick SiON film and a 0.1 μm thick SiO_2 film onto a silicon wafer covered by 6 μm thick thermal oxide. During deposition, hydrogen bonds of Si–H, N–H, and Si–O–H are incorporated into the film. They cause absorption in the wavelength range from 1.4 to 1.55 μm. High-temperature annealing is necessary to break the hydrogen bonds and achieve low-loss optical waveguides [26]. We pre-anneal the sample at 950 °C for 24 h. Then the waveguide pattern is written by electron beam lithography (JEOL JBX6300-FS). The sample is etched in an inductively coupled plasma reactive ion etching (ICP-RIE) chamber (Oxford Instruments Plasmalab 100) using gases CHF_3 and O_2. The ICP-RIE process produces very smooth

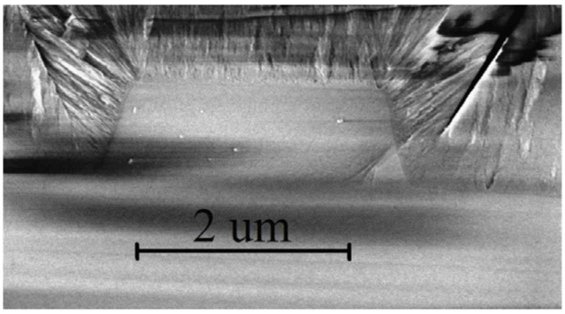

Figure 2. SEM image of the facet of the waveguide taper after 1100 °C annealing. The scale bar is 2 μm. The designed width of the taper is 3 μm. The final width shrinks after processing.

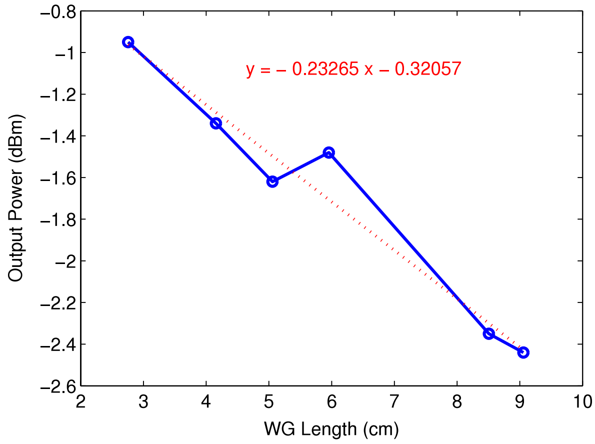

Figure 3. Output power of the waveguides as a function of the length of the waveguides. Propagation loss is estimated by linearly fitting the experimental data.

surfaces while still maintaining reasonably steep side walls. After removing the residual resist, a 2 μm thick SiO_2 layer is deposited by PECVD. Note that for the bottom cladding, a very thick SiO_2 layer is needed to prevent leaky propagation because the silicon substrate has a substantially higher refractive index than SiON. For the top cladding, a moderately thick layer suffices to guard the core since air has a lower refractive index than SiON. The fabricated waveguides have a width of 2.3 μm and a height of 0.9 μm for single mode operation at around $\lambda = 1.55$ μm. The ends of the waveguides are linearly tapered to $W = 3$ μm for better light coupling. Finally the sample is cleaved and annealed at 1100 °C for 24 h. This annealing not only removes the hydrogen bonds but also smooths the SiO_2 and SiON interface. Both effects contribute to reducing the propagation loss even further. An SEM image of the waveguide facet after annealing is shown in figure 2.

4. Optical testing

For loss measurements, eight waveguides are fabricated on one chip. There are six waveguides, each of which contains eight identical 90° bends. The bending radius is 1 mm. The lengths of these waveguides range from 2.76 to 9.06 cm. In addition, two straight waveguides are fabricated on the same chip to analyze the bending loss. We use a tunable laser (HP 8168F) as the light source. Light is coupled into a waveguide in the TE polarization via two lensed fibers with a mode diameter of 2.5 μm. First, we measure the output power of the waveguide as a function of the waveguide's length at $\lambda = 1.574$ μm. The propagation loss is found to be 0.23 dB cm^{-1} by linearly fitting the experimental data, as shown in figure 3. Second, we perform a wavelength scanning for all the waveguides from 1.5 to 1.574 μm. By fitting the spectral data using $P = \alpha L + C_0$ at each wavelength, we can separate the propagation loss α from the coupling loss C_0. The results are shown in figure 4.

We can still see an absorption peak around 1.5 μm, indicative of residual N–H bonds after the high temperature annealing. Comparison of the transmission between the straight waveguides and those curved waveguides shows that

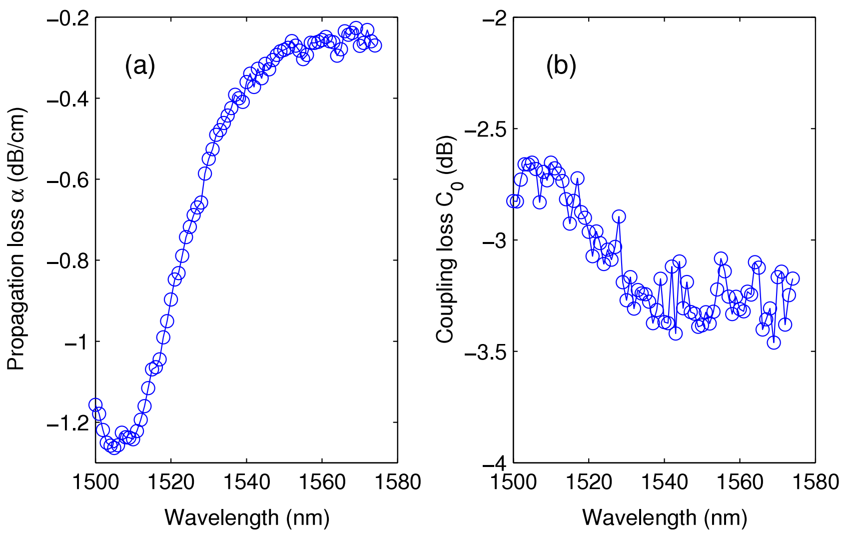

Figure 4. Spectral dependence of (a) propagation loss and (b) coupling loss obtained from a chip containing eight waveguides.

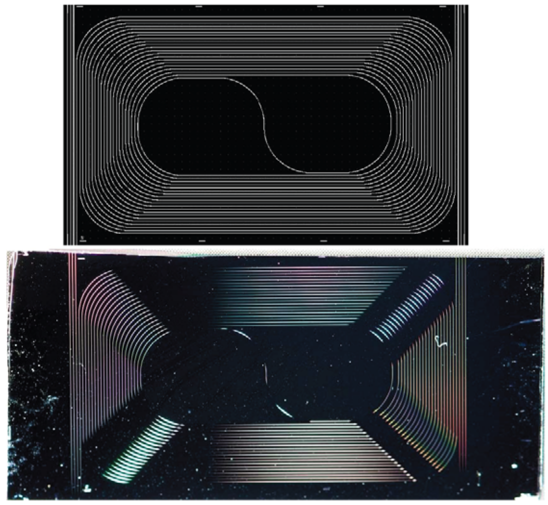

Figure 5. (a) Design and (b) image of a spiral waveguide sample. The pattern size is 2.6 cm × 1.5 cm.

the bending loss is very low (below our detection limit). The estimated loss based on bending loss theory [27] is below 0.003 dB/90° bend. The coupling loss is quite stable, varying within 0.8 dB in the spectrum window. On average the coupling loss is around 1.6 dB per facet from 1.54 to 1.57 μm. Considering the mismatch between the lensed fiber mode diameter and the waveguide facet height, this indicates that the facets are reasonably good after simple cleaving. We perform the optical testing before annealing at 1100 °C for 24 h also. Comparing the results before and after the last annealing, the propagation loss is reduced from about 1 to 0.23 dB cm^{-1} at 1.574 μm. This can be attributed to the fact that annealing helps to smooth the sidewall roughness at the interface between the SiON core and SiO_2 cladding and further remove the hydrogen bonds. This post-fabrication annealing is critical to achieving sufficiently low loss despite substantially smaller waveguide cross-section than previously reported SiON waveguides. Note that the low-loss SiON waveguides reported here have a 2 μm top cladding whereas SiON waveguides reported previously [23, 24] had top cladding thicker than 5 μm. Also, the bottom cladding is only 6 μm thick instead of 8–10 μm thick as reported in the previous paper. With the balanced choice of SiON refractive index demonstrated here, the reduction of both the core and cladding dimensions produces a substantially smaller overall cross-section. The reduction of top cladding thickness not only significantly reduces the processing (SiO_2 PECVD) time but may also help improve the performance of active SiON devices. For example, the power consumption of a thermo-optic SiON switch or tunable filter will decrease as the waveguide cross-section (or heating volume) decreases.

5. Meter-long spiral waveguide

We further design a spiral waveguide with a total length of 118 cm and a universal bending radius of 3 mm. A picture of a fabricated sample is shown in figure 5. We also include six straight waveguides on the chip for analyzing the propagation and coupling losses.

After the fabrication, we measure the insertion loss of the straight waveguides and spiral waveguide with the same setup. The spectral dependences of propagation loss and coupling loss for this chip are obtained as shown in figure 6. The propagation loss is 0.47 dB cm^{-1} at 1.57 μm. The loss is higher than shorter waveguides because longer waveguides are more likely to see accidental defects. (Note that part of the fabrication process is completed in a room with inadequately filtered ambient air, which tends to bring in small particles.) As FDFD simulation gives a group index of 1.555 for the TE mode, this meter-long waveguide can offer a temporal delay up to 6.1 ns. Considering the loss for the short and spiral waveguides, the dependence of temporal delay on propagation loss is around 0.11–0.23 ns/dB at 1.57 μm.

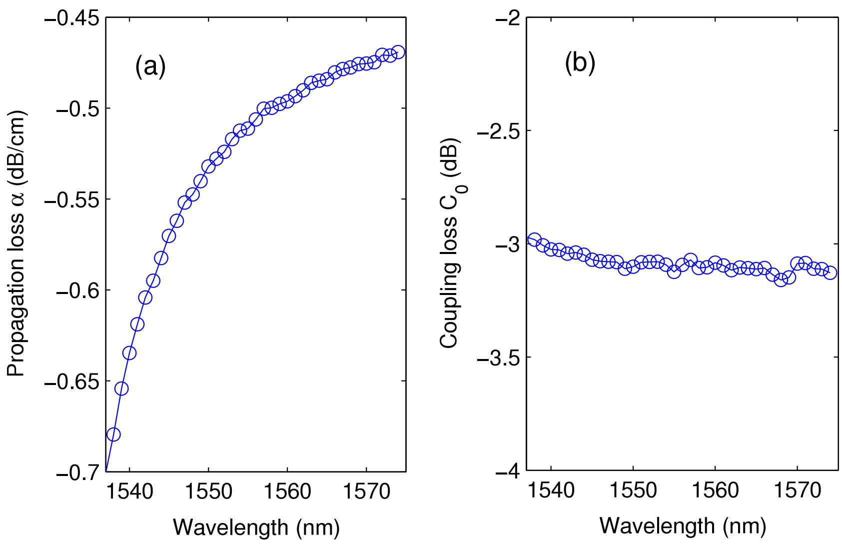

Figure 6. Spectral dependence of (a) propagation loss and (b) coupling loss of the spiral waveguide.

To further analyze the loss, it is helpful to note that the propagation loss of an optical waveguide can be attributed to scattering by defects or roughness and material absorption. E-beam lithography is employed in this work to minimize lithography-induced structure imperfection/roughness and help to reduce scattering loss. Note that ordinary UV photolithography available in academic cleanrooms uses relatively long wavelengths (e.g. 365 nm), with relatively low-resolution photomasks patterned by laser direct-write, and low-resolution photoresists. For high-throughput production in industry, high-resolution deep UV (DUV) lithography (e.g. at 193 nm) may be used, with high-performance DUV photoresists and high-quality DUV photomasks, which are patterned by high-resolution e-beam lithography. Using e-beam lithography in this work allows us to emulate, in academic cleanrooms, the high-performance industrial DUV lithography capability (22 nm features and <3 nm critical dimension control [28]). Note that, in this work, delay lines are investigated primarily for phased array antenna (PAA) applications [13]. For such applications, there is little restriction on the wavelength choice. Therefore, we can choose wavelengths greater than 1570 nm to obtain minimal absorption loss. For fiber-optic communications, further efforts would be needed to reduce the residual absorption loss in the C-band. Prior research has shown that it is possible to reduce the absorption peak to about 0.1 dB cm^{-1} through more sophisticated annealing schemes [22]. Adjusting the gas flow ratio r to tune the SiON composition may also help, although this is constrained by our interest of maintaining an index difference around 0.1 to balance the waveguide cross-sectional area, propagation loss, and bending size. As e-beam lithography and annealing are employed in this work to help minimize the roughness-induced scattering and absorption, the residual loss observed at wavelengths greater than 1570 nm is largely due to the ambient cleanness issues, which are limited by the facilities accessible to us. Note that the coupling loss can potentially be further improved through ingenious mode converters [29], although the current coupling loss level is not uncommon for delay lines in phased array antennas [13].

6. Conclusion

In this work, we have investigated SiON waveguides in a design regime that can offer a compact footprint and low loss for long optical delay lines. With the choice of a moderately low refractive index contrast on the order of 0.1, a balance can be achieved among small waveguide cross-section, low propagation loss, and small bending loss in a reasonably small bending radius. High temperature annealing for SiON is performed after deposition of the top cladding. As such, this annealing not only removes light absorbing bonds in the materials, but also smooths the core–cladding interface. This post-fabrication annealing and the precision e-beam lithography contribute to reducing the sidewall roughness and the associated scattering loss in SiON waveguides. With excellent compatibility with silicon photonics, SiON waveguides studied here can potentially be used for delay lines of an on-chip switchable delay network for phased array antennas. The stronger confinement achieved in the smaller waveguide cross-section will offer advantages for high-density integration of such delay lines including potential 3D integration by transfer printing [30]. Lastly, the reduced SiON waveguide cross-section may also help improve the performance of active (e.g. thermo-optic) SiON devices.

Acknowledgments

The authors are grateful to Leonard C Feldman, Ryan A Integlia, and Ying Qian for helpful discussions. This work is supported in part by AFOSR grant No FA9550-08-1-0394 (G Pomrenke). This research is carried out in part at the Center for Functional Nanomaterials, Brookhaven National Laboratory, which is supported by the US Department of Energy, Office of Basic Energy Sciences, under contract No DE-AC02-98CH10886.

References

[1] Lipson M 2005 Guiding, modulating, and emitting light on silicon—challenges and opportunities *J. Lightwave Technol.* **23** 4222–38
[2] Soref R A 2006 The past, present, and future of silicon photonics *IEEE J. Sel. Top. Quantum Electron.* **12** 1678–87
[3] Jalali B and Fathpour S 2006 Silicon photonics *J. Lightwave Technol.* **24** 4600–15
[4] Liu A S, Jones R, Liao L, Samara-Rubio D, Rubin D, Cohen O, Nicolaescu R and Paniccia M 2004 A high-speed silicon optical modulator based on a metal–oxide–semiconductor capacitor *Nature* **427** 615–8
[5] Xu Q F, Schmidt B, Pradhan S and Lipson M 2005 Micrometre-scale silicon electro-optic modulator *Nature* **435** 325–7
[6] Gu L L, Jiang W, Chen X N, Wang L and Chen R T 2007 High speed silicon photonic crystal waveguide modulator for low voltage operation *Appl. Phys. Lett.* **90** 071105
[7] Kang Y M *et al* 2009 Monolithic germanium/silicon avalanche photodiodes with 340 GHz gain-bandwidth product *Nature Photon.* **3** 59–63
[8] Assefa S, Xia F and Vlasov Y A 2010 Reinventing germanium avalanche photodetector for nanophotonic on-chip optical interconnects *Nature* **464** 80–4
[9] Liu J, Sun X, Camacho-Aguilera R, Kimerling L C and Michel J 2010 Ge-on-Si laser operating at room temperature *Opt. Lett.* **35** 679–81
[10] Boyraz O and Jalali B 2004 Demonstration of a silicon Raman laser *Opt. Express* **12** 5269–73
[11] Lee J Y, Yin L, Agrawal G P and Fauchet P M 2010 Ultrafast optical switching based on nonlinear polarization rotation in silicon waveguides *Opt. Express* **18** 11514–23
[12] Matthews P J, Frankel M Y and Esman R D 1998 A wide-band fiber-optic true-time-steered array receiver capable of multiple independent simultaneous beams *IEEE Photon. Technol. Lett.* **10** 722–4
[13] Chen M Y, Subbaraman H and Chen R T 2008 Photonic crystal fiber beamformer for multiple x-band phased-array antenna transmissions *IEEE Photon. Technol. Lett.* **20** 375–7
[14] Xia F N, Sekaric L and Vlasov Y 2007 Ultracompact optical buffers on a silicon chip *Nature Photon.* **1** 65–71
[15] LeGrange J D, Simsarian J E, Bernasconi P, Buhl L, Gripp J and Neilson D T 2009 Demonstration of an

integrated buffer for an all-optical packet router *IEEE Photon. Technol. Lett.* **21** 781–3

[16] Park H, Mack J P, Blumenthal D J and Bowers J E 2008 An integrated recirculating optical buffer *Opt. Express* **16** 11124–31

[17] Bauters J F, Heck M J R, John D D, Barton J S, Bruinink C M, Leinse A, Heideman R G, Blumenthal D J and Bowers J E 2011 Planar waveguides with less than 0.1 dB/m propagation loss fabricated with wafer bonding *Opt. Express* **19** 24090–101

[18] Bauters J F, Heck M J R, John D D, Dai D, Tien M-C, Barton J S, Leinse A, Heideman R G, Blumenthal D J and Bowers J E 2011 Ultra-low-loss high-aspect-ratio Si_3N_4 waveguides *Opt. Express* **19** 3163–74

[19] Payne F P and Lacey J P R 1994 A theoretical analysis of scattering loss from planar optical waveguides *Opt. Quantum Electron.* **26** 977–86

[20] Song W, Integlia R A and Jiang W 2010 Slow light loss due to roughness in photonic crystal waveguides: an analytic approach *Phys. Rev.* B **82** 235306

[21] Gondarenko A, Levy J S and Lipson M 2009 High confinement micron-scale silicon nitride high Q ring resonator *Opt. Express* **17** 11366–70

[22] Bona G-L, Germann R and Offrein B J 2003 SiON high refractive-index waveguide and planar lightwave circuits *IBM J. Res. Dev.* **47** 239–49

[23] Worhoff K, Roeloffzen C G H, De Ridder R M, Driessen A and Lambeck P V 2007 Design and application of compact and highly tolerant polarization-independent waveguides *J. Lightwave Technol.* **25** 1276–83

[24] Fadel M, Bülters M, Niemand M, Voges E and Krummrich P M 2009 Low-loss and low-birefringence high-contrast silicon-oxynitride waveguides for optical communication *J. Lightwave Technol.* **27** 698–705

[25] Fallahkhair A B, Li K S and Murphy T E 2008 Vector finite difference mode-solver for anisotropic dielectric waveguides *J. Lightwave Technol.* **26** 1423–31

[26] Denisse C M M, Troost K Z, Habraken F H P M, van der Weg W F and Hendriks M 1986 Annealing of plasma silicon oxynitride films *J. Appl. Phys.* **60** 2543–7

[27] Snyder A W and Love J D 1983 *Optical Waveguide Theory* (London: Chapman and Hall)

[28] *International Technology Roadmap for Semiconductors* 2011 edn Lithography Tables, www.itrs.net

[29] Spuhler M M, Offrein B J, Bona G L, Germann R, Massarek I and Erni D 1998 A very short planar silica spot-size converter using a nonperiodic segmented waveguide *IEEE J. Lightwave Technol.* **16** 1680–5

[30] Ahn J H, Kim H S, Lee K J, Jeon S, Kang S J, Sun Y G, Nuzzo R G and Rogers J A 2006 Heterogeneous three-dimensional electronics by use of printed semiconductor nanomaterials *Science* **314** 1754–7